

Measuring the tendency of CNNs to Learn Surface Statistical Regularities

Jason Jo
 MILA, Université de Montréal
 IVADO
 jason.jo.research@gmail.com

Yoshua Bengio
 MILA, Université de Montréal
 CIFAR
 yoshua.umontreal@gmail.com

Abstract

Deep CNNs are known to exhibit the following peculiarity: on the one hand they generalize extremely well to a test set, while on the other hand they are extremely sensitive to so-called adversarial perturbations. The extreme sensitivity of high performance CNNs to adversarial examples casts serious doubt that these networks are learning high level abstractions in the dataset. We are concerned with the following question: How can a deep CNN that does not learn any high level semantics of the dataset manage to generalize so well? The goal of this article is to measure the tendency of CNNs to learn surface statistical regularities of the dataset. To this end, we use Fourier filtering to construct datasets which share the exact same high level abstractions but exhibit qualitatively different surface statistical regularities. For the SVHN and CIFAR-10 datasets, we present two Fourier filtered variants: a low frequency variant and a randomly filtered variant. Each of the Fourier filtering schemes is tuned to preserve the recognizability of the objects. Our main finding is that CNNs exhibit a tendency to latch onto the Fourier image statistics of the training dataset, sometimes exhibiting up to a 28% generalization gap across the various test sets. Moreover, we observe that significantly increasing the depth of a network has a very marginal impact on closing the aforementioned generalization gap. Thus we provide quantitative evidence supporting the hypothesis that deep CNNs tend to learn surface statistical regularities in the dataset rather than higher-level abstract concepts.

1. Introduction

The generalization ability of a machine learning model can be measured by evaluating its accuracy on a withheld test set. For visual learning tasks, convolutional neural networks (CNNs) [21] have become the de facto machine learning model. These CNNs have achieved record breaking object recognition performance for the CIFAR-10 [1], SVHN [26] and ImageNet [34] datasets, at times surpassing human performance [13]. Therefore, on the one hand,

very deep CNN architectures have been designed which obtain very good generalization performance. On the other hand, it has been shown that these same CNNs exhibit an extreme sensitivity to so-called *adversarial examples* [40]. These adversarial examples are perceptually quite similar to the original, “clean” image. Indeed humans are able to correctly classify the adversarial image with relative ease, whereas the CNNs predict the wrong label, usually with very high confidence. *The sensitivity of high performance CNNs to adversarial examples casts serious doubt that these networks are actually learning high level abstract concepts [6, 27]*. This begs the following question: *How can a network that is not learning high level abstract concepts manage to generalize so well?*

Roughly speaking, there are two ways in which a machine learning model can generalize well. The first way is *the ideal way*: the model is trained in a manner that captures high level abstractions in the dataset. The second way is less than ideal: *the model has a tendency to overfit to superficial cues that are actually present in both the train and test datasets*; thus the statistical properties of the dataset plays a key role. In this fashion, high performance generalization is possible without actually explicitly learning any high level concepts.

In Section 2 we discuss the generalization ability of a machine learning model and its relation to the surface statistical regularities of the dataset. In particular, by drawing on computer vision literature on the statistics of natural images, we believe that it is possible for natural image train and test datasets to share *many superficial cues*. This leads us to postulate our main hypothesis: *the current incarnation of deep neural networks has a tendency to learn surface statistical regularities in the dataset*. In Section 3 we discuss related work.

To test our hypothesis, we will quantitatively measure this tendency. To this end, for a dataset X it is sufficient to construct a perturbation map F :

$$F : X \mapsto X', \tag{1}$$

which satisfies the following properties:

1. *Object Recognizability is preserved.* Given a clean image $x \in X$ and its perturbation $x' \in X'$, the recognizability of the object in the images x and x' is almost exactly preserved from the perspective of a human. This guarantees that X, X' share the same high level concepts.
2. *Qualitatively Different Surface Regularities.* While the recognizability of the objects is roughly preserved by the perturbation map F , the datasets X and X' also exhibit qualitatively different image statistics. In combination with the first property, this guarantees that the two datasets X, X' share the same high level abstractions but may exhibit different superficial cues.
3. *Existence of a non-trivial generalization gap.* Given the clean dataset $\{(X_{\text{train}}, Y_{\text{train}}), (X_{\text{test}}, Y_{\text{test}})\}$, the map F produces another dataset $\{(X'_{\text{train}}, Y_{\text{train}}), (X'_{\text{test}}, Y_{\text{test}})\}$. Now we simply measure the test accuracy of a deep CNN trained on either X_{train} or X'_{train} on both X_{test} and X'_{test} and compute the corresponding generalization gap. A good perturbation map F is one in which the generalization gap is non-trivial.

In Section 4, we show that a natural candidate for these maps F are maps which are defined by Fourier filtering. We define two types of Fourier filtering schemes: radial and random. Each of these schemes has a parameter that needs to be tuned: for the radial filter we must define the radius of the mask, and for the random filter we must define the probability of setting a Fourier mode to zero in a uniformly random fashion. We will present our tuned Fourier filter maps for the SVHN and CIFAR-10 datasets. In addition we present visual evidence that the recognizability of the objects in the filtered datasets is extremely robust to the human eye. Due to the fact that we are Fourier filtering, the filtered datasets will by construction exhibit different image statistics. Thus we are able to produce filtered/perturbed training and test datasets which share the same high level perceptual content as the original datasets but exhibit qualitatively different surface statistical regularities, *e.g.* the Fourier image statistics.

In Section 5 we present generalization experiments which are designed to test our main hypothesis. High performance CNNs are trained on one of the $\{X_{\text{unfiltered}}, X_{\text{radial}}, X_{\text{random}}\}$ datasets and the test accuracy is evaluated on *all* the other test distributions. We show a general pattern of the deep CNN models exhibiting a tendency to latch onto the surface statistical regularities of the training dataset, sometimes exhibiting up to a 28% gap in test accuracy. Another striking result was that CNNs trained on $X_{\text{unfiltered}}$ generalized quite poorly to X_{radial} , to which we report a generalization gap upwards of 18%. Moreover, increasing the depth of the CNN in a significant

manner (going from 92 layers to 200 layers) has a very small effect on closing the generalization gap.

Our last set of experiments involves training on the fully augmented training set, which now enjoys a variance of its Fourier image statistics. We note that this sort of data augmentation was able to close the generalization gap. However, we stress that it is doubtful that this sort of data augmentation scheme is sufficient to enable a machine learning model to truly learn the semantic concepts present in a dataset. Rather this sort of data augmentation scheme is analogous to adversarial training [40, 9]: there is a non-trivial regularization benefit, but it is not a solution to the underlying problem of not learning high level semantic concepts, nor do we aim to present it as such.

In Section 6 we present our conclusion that our empirical results provide evidence for the claim that the current incarnation of deep neural networks are not actually learning high level abstractions. Finally we highlight promising new research directions towards this goal.

2. Generalization and Surface Statistical Regularities

In this section we wish to reconcile two seemingly inharmonious yet individually valid (in their respective contexts) claims about the generalization properties of deep CNNs:

1. *Claim #1:* Deep CNNs are generalizing extremely well to an unseen test set.
2. *Claim #2:* General sensitivity to adversarial examples show that deep CNNs are not truly capturing abstractions in the dataset.

One key intuition to understand the above two claims is to recognize that there is actually a strong statistical relationship between image statistics and visual understanding. For example [43] explored the relationship between image statistics and visual scene categorization. They were actually able to use image statistics to predict the presence or absence of objects in an image of a natural scene. In [31], the authors placed synthetic, rendered objects into statistically unlikely to occur yet natural looking backgrounds. For example Figure 2 of [31] depicts a car floating at an angle in a grassy area with clouds in the background. They then used these synthetic images to test the invariance of various visual features for object recognition, one example being the sensitivity of object recognition to covariation with the background. To this end, they hypothesize that computer vision algorithms may “...lean heavily on background features to perform categorization.”

Therefore, when the training and test set share similar image statistics, it is wholly possible for a machine learning model to learn superficial cues and generalize well, albeit in a very narrow sense as they are highly dependent on the

image statistics. Adversarial examples would be destroying the superficial cues. We believe that this is precisely how deep CNNs can attain record breaking generalization performance on all sorts of natural image tasks, and yet can be so sensitive to adversarial perturbations. Most importantly, the above reasoning can explain how a machine learning model can actually generalize well without ever having to explicitly learn abstract concepts. To this end, we formally state our main hypothesis:

The current incarnation of deep neural networks exhibit a tendency to learn surface statistical regularities as opposed to higher level abstractions in the dataset. For tasks such as object recognition, due to the strong statistical properties of natural images, these superficial cues that the deep neural network have learned are sufficient for high performance generalization, but in a narrow distributional sense.

Having stated our main hypothesis, we feel the need to stress that it is not fair to compare the generalization performance of CNN to a human being. In contrast to a CNN, a human being is exposed to an incredibly diverse range of lighting conditions, viewpoint variations, occlusions, among a myriad of other factors.

3. Related Work

To the best of our knowledge, we are the first to consider using Fourier filtering for the purpose of measuring the tendency of CNNs to learn surface statistical regularities in the dataset. With respect to related work, we highlight [17] which showed that CNNs trained on the clean MNIST, CIFAR-10 and GTSRB [39] datasets generalize quite poorly to the so-called “negative” test sets, where the test images have negated brightness intensities. The major difference from [17] and our work is that negative images are known to be more challenging for the task of object recognition for human beings, we refer to [12, 30, 8, 29] and the numerous references therein. Indeed from [12] we quote: “...negative images containing low-frequency components were considerably more difficult to recognize than the corresponding positive images.” From [7, 4], we know that natural images tend to have the bulk of their Fourier spectrum concentrated on the low to mid range frequencies. To this end, we view our Fourier filtering scheme as a better principled scheme than image negation with respect to preserving the recognizability of the objects. Finally [17] employs CNN models for the CIFAR-10 which attain a maximum test accuracy of about 84% while we use a more modern and up to date CNN model, regularly achieving 95% test accuracy for the CIFAR-10, much closer to the current state of the art.

The problems of transfer learning [44, 37, 38] and domain adaptation [35, 10] both investigate the generalization ability of deep neural networks. However we believe the more relevant research literature is coming from adversarial examples. Originally introduced and analyzed for the MNIST dataset in [40], adversarial examples have sparked a flurry of research activity. The original work [40] showed that it is not only possible to generate adversarial examples which fool a given network, these adversarial examples actually *transfer* across different network architectures. [9] further explored the transferability of adversarial examples for the MNIST and CIFAR-10 datasets, and [23] was able to show the existence of a universal adversarial noise for ImageNet dataset. The universal adversarial noise is image agnostic, e.g. is able to be applied to a wide range of images and still fool various networks.

As a response to these adversarial examples, there have been various attempts to increase the robustness of deep neural networks to adversarial perturbations. [28] employed defensive-distillation. [11] used so-called contractive networks. Moreover, [11] posited that the core problem with adversarial examples emanates from the current training setup used in deep learning, rather than the network architecture. Along these lines, [5] obtained promising results by modifying the training regime of SGD by forcing the convolutional layers to be approximate Parseval tight frames [19]. This method led to state of the art performance on the CIFAR-10/100 as well as the SVHN dataset while also increasing the robustness of the network to adversarial examples. Similarly in [33] the training loop is modified to improve robustness to adversarial examples. Specifically [33] modifies SGD by rescaling the batch gradients and reports an increased robustness to adversarial examples for the MNIST and CIFAR-10 datasets, though the CIFAR-10 models suffer a non-trivial degradation in clean test accuracy.

The most popular adversarial robustness method has been adversarial training [9, 22, 24, 36, 40, 20]. Adversarial training methods all rely on data augmentation: the training data set is augmented with adversarial examples. In general we comment that these methods tend to rely on a certain adversarial example generation technique. Thus these methods are not guaranteed to be robust to adversarial examples generated from some alternate method. To this end, [6, 27] cast doubt that supervised CNNs are actually learning semantic concepts in the datasets.

4. Robustness of Object Recognition to Fourier Filtering

The surface statistical regularities we will be concerned with are the Fourier image statistics of a dataset. While natural images are known to exhibit a huge variance in the raw pixel space, it has been shown [7, 4] that the Fourier im-

age statistics of natural images obey a power law decay: the power $P(w)$ of a Fourier mode (also referred to as a frequency) w decays $\propto \frac{A}{|w|^{2-\eta}}$ for some A and η which varies over the image types, but η is typically small. An immediate takeaway is that natural images tend to have the bulk of their Fourier spectrum concentrated in the low to medium range frequencies. *Due to this power law concentration of energy in the frequency space, it is possible to perform certain types of Fourier filtering and preserve much of the perceptual content of an image.*

In this section we define our Fourier filtering setup and present visual evidence that while the Fourier filtering process does indeed introduce artifacts and does degrade the quality of the image, the recognizability of the objects in the image is still quite robust from a human point of view. For a given dataset (X, Y) (which can represent either the train or test dataset), we have the following:

- (X, Y) itself, the *unfiltered* version.
- (X_{radial}, Y) , the *low frequency filtered* version. We use a radial mask in the Fourier domain to set higher frequency modes to zero.
- (X_{random}, Y) , the *randomly filtered* version. We use a random mask which uniformly at random sets a Fourier mode to zero with probability p . The random mask is generated once and applied to all the elements of X .

Let $X \in \mathbb{R}^{H \times W}$ denote a $H \times W$ shaped image with only 1 color channel. Recall that the 2D Discrete Fourier Transform (DFT) [3] of X , denoted $\mathcal{F}(X)$ is defined as:

$$\mathcal{F}(X)[k, l] := \frac{1}{\sqrt{HW}} \sum_{h=0}^{H-1} \sum_{w=0}^{W-1} X[w, h] e^{-j2\pi(\frac{wk}{W} + \frac{lh}{H})}, \quad (2)$$

for $k = 0, \dots, W-1, l = 0, \dots, H-1$, and $j = \sqrt{-1}$. If X is an RGB image, so it has $C = 3$ channels, we then compute the DFT for each image channel. We will furthermore consider the *shifted DFT* in which the DC component is located in the center of the $H \times W$ matrix as opposed to the $(0, 0)$ index. We let $\mathcal{F}^{-1}(X)$ denote the inverse FFT of X , composed with the appropriate inverse spectral shift.

In this article, we will consider two types of Fourier filtering schemes:

- *Radial masking*. This scheme is parameterized by the mask radius r . We will require that each of our images X have height H and width W of even length. The radial mask M_r is defined as:

$$M_r[i, j] := \begin{cases} 1 & \text{if } \|(i, j) - (W/2, H/2)\|_{\ell_2} \leq r, \\ 0 & \text{otherwise.} \end{cases} \quad (3)$$

We use $\|x - y\|_{\ell_2}$ to denote the ℓ_2 distance between the vectors x and y . The mask M_r is applied across the channels.

For an unfiltered dataset X , we define X_{radial} as:

$$X_{\text{radial}} := \mathcal{F}^{-1}(\mathcal{F}(X) \circ M_r), \quad (4)$$

where \circ denotes the element-wise *Hadamard product*.

- *Uniformly random masking*. This scheme is parameterized by a drop probability p . We will generate a random mask M_p once, and then apply the same random mask to each of the DFTs. The mask M_p is defined as:

$$M_p[c, i, j] := \begin{cases} 0 & \text{with probability } p, \\ 1 & \text{otherwise.} \end{cases} \quad (5)$$

Note that we do not have the same random mask per channel. For an unfiltered dataset X , we define X_{random} as:

$$X_{\text{random}} := \mathcal{F}^{-1}(\mathcal{F}(X) \circ M_p), \quad (6)$$

For the rest of the section we will present which mask radius and random masking probability hyperparameters were used for the SVHN and CIFAR-10 natural image datasets. Note that we did not use the MNIST dataset due to its extreme sparsity which results in very low recognizability of the digits after Fourier filtering.

4.1. SVHN



Figure 1: The first image in each column corresponds to the Fourier mask in frequency space. A white pixel corresponds to preserving the Fourier mode, black/color corresponds to setting it to zero. **Top row:** No Fourier filtering applied, original SVHN images. **Middle row:** Radial mask and the corresponding filtered images. **Bottom row:** Random mask and the corresponding filtered images. Best viewed in color.

For the SVHN dataset, the images have spatial shape $(32, 32)$ with 3 color channels corresponding to RGB. For the radial masking we used a mask radius of 4.25 and for random masking we used $p = 0.1$. In Figure 1 we show the masks and a comparison between unfiltered and filtered images. We notice that while both the radial and random filters produce some visual artifacts, and some random masks can actually result in noticeable color distortions, the overall recognizability of the digits is quite robust.

4.2. CIFAR-10



Figure 2: The first image in each column corresponds to the Fourier mask in frequency space. A white pixel corresponds to preserving the Fourier mode, black/color corresponds to setting it to zero. **Top row:** No Fourier filtering applied, original CIFAR-10 images. **Middle row:** Radial mask and the corresponding filtered images. **Bottom row:** Random mask and the corresponding filtered images. Best viewed in color.

For the CIFAR-10, the images have spatial shape (32, 32) with 3 color channels corresponding to RGB. For the radial masking we used a mask radius of 11.0 and for random masking we used $p = 0.1$. In Figure 2 we show the masks and a comparison between unfiltered and filtered images. Observe that while there are undoubtedly artifacts that arise from our Fourier filters, the recognizability of the objects is quite robust to the human eye. Furthermore, the artifacts that do occur have a tendency to actually occur *in the background of the image* or cause minimal degradation to the recognizability of the object. Refer to the Supplementary Materials for more visual examples.

5. Generalization Experiments

In this section we present our generalization experiments. Our generalization experiments consists of the following: for the CIFAR-10 and SVHN datasets, we take some established high-performance CNN architectures (while they are not state of the art, they are typically very close to state of the art performance) and train them on one of the following: $\{X_{\text{train}}^{\text{unfiltered}}, X_{\text{train}}^{\text{radial}}, X_{\text{train}}^{\text{random}}\}$ and then test the accuracy of each of these trained models on *all* of the following test sets $\{X_{\text{test}}^{\text{unfiltered}}, X_{\text{test}}^{\text{radial}}, X_{\text{test}}^{\text{random}}\}$. We refer to a *test gap* or a *generalization gap* as the maximum difference of the accuracy on the various test sets. For the CIFAR-10 and SVHN datasets, we use exactly the parameterized Fourier filtering setups from Section 4.

For both the SVHN and CIFAR-10 experiments we trained a Preact ResNet [15] with Bottleneck architecture of depth 92 and 200 using the so-called “HeNormal” initialization from [14], using a random seed of 0. For format-

ting purposes, we only show graphical plots for the very deepest highest performance (Preact-ResNet-200) model and merely summarize the Preact-ResNet-92 models performance in a table. We include the full graphical plots for the depth 92 model in the Supplementary Materials.

In general, none of the training sets generalized universally well to the various test sets. So we also trained on the fully augmented training set:

$$X_{\text{train}}^{\text{augmented}} := X_{\text{train}}^{\text{unfiltered}} \cup X_{\text{train}}^{\text{radial}} \cup X_{\text{train}}^{\text{random}} \quad (7)$$

and then measured the generalization performance on the various test sets.

5.1. SVHN Experiments

For the SVHN dataset we follow the convention of [45]: we combine the original training set and the extra dataset to form a new training set and we normalize all the pixel intensities to [0,1] by dividing all the values by 255.0. Otherwise, no other form of data augmentation or pre-processing was used.

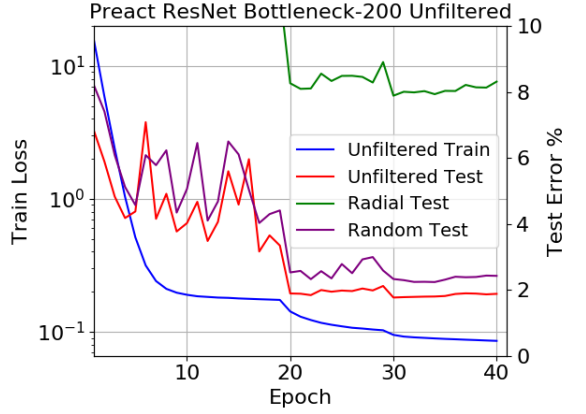
We train the ResNets for 40 epochs using Nesterov momentum [25] with an initial learning rate of 0.01 with momentum parameter 0.9. The training batchsize was 128, the L2 regularization parameter was 0.0005 and we decayed the learning rate at epochs 20 and 30 by dividing by 10.

In Figure 3 we present the generalization plots for the Preact-ResNet-200 trained on the unfiltered, randomly filtered and radially filtered training sets. In Figure 4 we present the graphical plot of the generalization curves for the Preact-ResNet-200 trained on the fully augmented training set. Finally in Figure 5 we present the SVHN generalization error table for both the Preact-ResNet-92 and the Preact-ResNet-200 model.

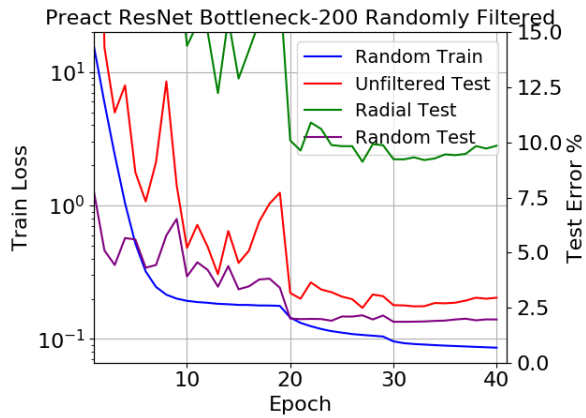
From these figures we observe that when trained on the unfiltered data and tested on the radially filtered test data, the networks exhibited a generalization gap of about 6.4%. Furthermore, when the nets were trained on the randomly filtered data, these networks had the worst generalization gap at approximately 7.89%, again for the radially filtered test set. Training on the radially filtered dataset seems to enjoy a regularization benefit with respect to the unfiltered test set, actually generalizing nearly 1.5% better on the unfiltered test set than the radially filtered test set. We observe that the networks trained on the radially filtered data tend to have the lowest generalization gap, and furthermore that training on the augmented training set reduced the generalization gap. One general theme was that regardless of the training set, depth seemed to have a negligible effect on closing the generalization gap.

5.2. CIFAR-10 Experiments

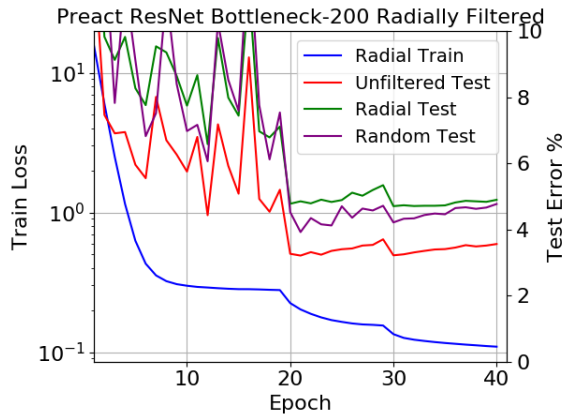
For the CIFAR-10 we perform global contrast normalization (zero-centering the training set and dividing by the



(a) Trained on Unfiltered SVHN



(b) Trained on Randomly Filtered SVHN



(c) Trained on Radially Filtered SVHN

Figure 3: Generalization plots for Preact-ResNet-Bottleneck-200 model. (a) Trained on unfiltered SVHN. (b) Trained on randomly filtered SVHN data. (c) Trained on radially filtered SVHN data. Best viewed in color.

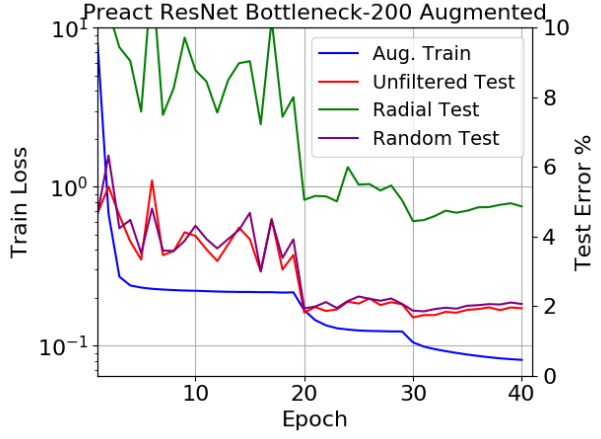


Figure 4: Augmented SVHN Training plots for ResNet-200. Best viewed in color.

Train/Test	Unfilt.	Radial	Random	Gen. Gap
Unfilt.	1.95%	8.41%	2.68%	6.46%
Radial	3.50%	5.07%	5.67%	2.17%
Random	4.01%	11.90%	2.04%	7.89%
Augmented	2.11%	5.06%	2.15%	2.95%

(a) Preact-ResNet-Bottleneck-92 SVHN Generalization

Train/Test	Unfilt.	Radial	Random	Gen. Gap
Unfilt.	1.88%	8.31%	2.42%	6.43%
Radial	3.56%	4.90%	4.77%	1.34%
Random	2.95%	9.85%	1.96%	7.89%
Augmented	1.94%	4.87%	2.06%	2.93%

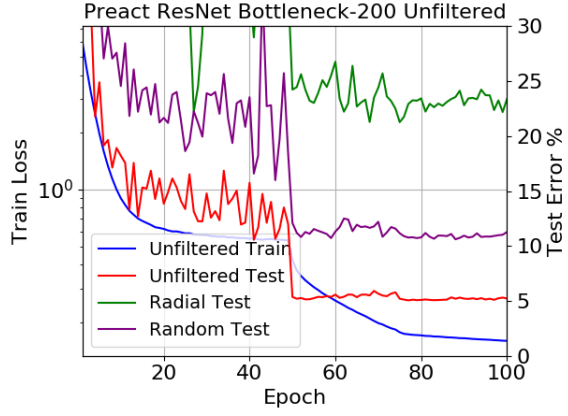
(b) Preact-ResNet-Bottleneck-200 SVHN Generalization

Figure 5: SVHN Generalization Table. The train indicates what the training set was, the test indicates the test set. Final test error is listed and the corresponding generalization gap.

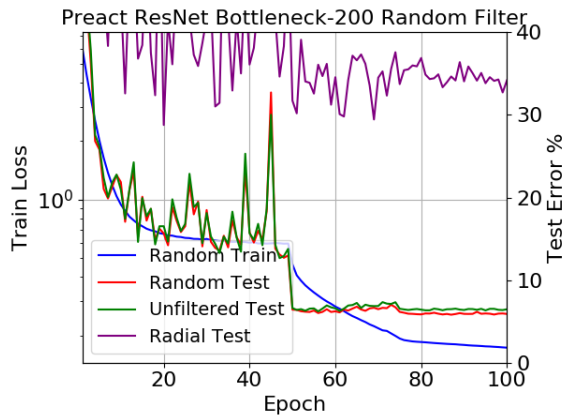
pixel-wise standard deviation) and augment via horizontal flips. During training we pad each 32x32 image with zeros to a 40x40 image and extract a random 32x32 crop.

We train the ResNets for 100 epochs with an initial learning rate of 0.01, which we boost up to 0.1 after 400 updates. The momentum parameter is 0.9. The training batchsize was 128, the L2 regularization parameter was 0.0001 and we decayed the learning rate at epochs 50 and 75 by dividing by 10. For the augmented models we trained a bit longer: 120 epochs with learning rate decays at epochs 60 and 80.

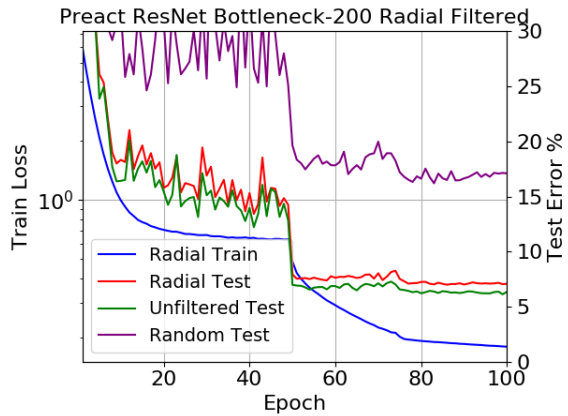
The CIFAR-10 generalization experiments otherwise are exactly the same setup as the SVHN generalization experiments from the previous section. In Figure 6 we present the generalization plots for the Preact-ResNet-200 trained on the unfiltered, randomly filtered and radially filtered train-



(a) Trained on Unfiltered CIFAR-10



(b) Trained on Randomly Filtered CIFAR-10



(c) Trained on Radially Filtered CIFAR-10

Figure 6: Generalization plots for Preact-ResNet-Bottleneck-200 model. (a) Trained on unfiltered CIFAR-10 data. (b) Trained on randomly filtered CIFAR-10 data. (c) Trained on radially filtered CIFAR-10 data. Best viewed in color.

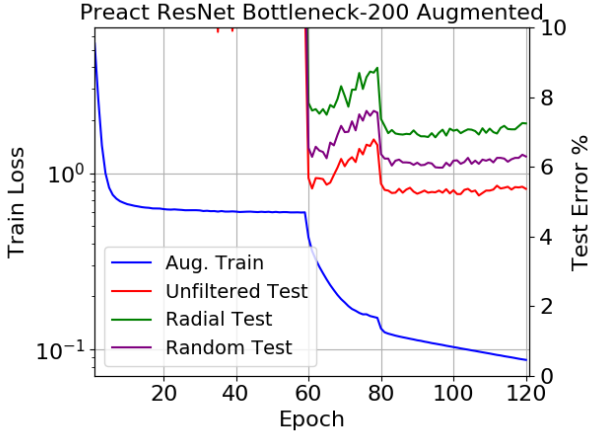


Figure 7: Preact-ResNet-200 trained on Fully Augmented CIFAR-10. Best viewed in color.

Train/Test	Unfilt.	Radial	Random	Gen. Gap
Unfilt.	5.54%	25.75%	12.31%	20.21%
Radial	6.91%	7.91%	18.45%	11.54%
Random	7.12%	35.03%	6.76%	28.27%
Augmented	5.85%	7.89%	6.74%	2.04%

(a) Preact-ResNet-Bottleneck-92 CIFAR-10 Generalization

Train/Test	Unfilt.	Radial	Random	Gen. Gap
Unfilt.	5.22%	23.37%	11.26%	18.15%
Radial	6.35%	7.07%	17.09%	10.74%
Random	6.47%	34.19%	5.9%	28.29%
Augmented	5.37%	7.25%	6.3%	1.88%

(b) Preact-ResNet-Bottleneck-200 CIFAR-10 Generalization

Figure 8: CIFAR-10 Generalization Table. The train indicates what the training set was, the test indicates the test set. Final test error is listed and the corresponding generalization gap.

ing sets. In Figure 7 we present the generalization plots for the Preact-ResNet-200 trained on the fully augmented CIFAR-10 dataset, and in Figure 8 we summarize all the exact error rates for the CIFAR-10 experiments.

From these figures we observe that when trained on the unfiltered data, the networks exhibited a generalization gap when tested on the radially filtered test set, of about 18–20%, much larger than the analogous gap for the SVHN dataset. Furthermore, when the nets were trained on the randomly filtered data, these networks again had the worst generalization gap at over 28%, again for the radially filtered test set. The networks trained on the radially filtered data tend to have the lowest generalization gap, and furthermore that training on the augmented training set reduces the generalization gap. Similar to the SVHN experimental results, depth seemed to have a negligible effect on closing

the generalization gap.

5.3. Discussion

We now wish to synthesize the experimental results presented in the previous sections. First we extend our claim that human object recognizability is robust to Fourier filtered image data to the claim that: the neural networks trained on the Fourier filtered datasets (both the radial and random filtered datasets) actually generalized quite well to the unfiltered test set. Indeed, from the tables in Figures 5 and 8, we highlight the fact that the nets that were trained on the random and radial datasets were only off by 1-2% of the best unfiltered test accuracy. This suggests that our choice of Fourier filtering schemes produced datasets that are perceptually not too far off from the original unfiltered dataset.

Despite the differences of the Fourier image statistics of the SVHN and CIFAR-10 datasets, as we noted previously, our SVHN and CIFAR-10 generalization experiments were of a nearly identical qualitative nature. We see that deep CNNs trained on an unfiltered natural image dataset exhibit a tendency to latch onto the image statistics of the training set, yielding a non-trivial generalization gap. The degree of this generalization gap can vary, ranging from 7-8% for the SVHN to over 18% for the CIFAR-10. Depth does not seem to have any real effect on reducing the observed generalization gaps. More generally, we note that there is no particular training set which generalizes universally well to all the test sets, though the radially filtered train set did tend to have the smaller generalization gap.

When training on the fully augmented training set, we observe an improvement in the generalization gap. However, we cast doubt on the notion that this sort of data augmentation scheme is sufficient to learn higher level semantic features in the dataset. Rather it is far more likely that the CNNs are learning a superficial robustness to the varying image statistics. To this end, we draw an analogy to adversarial training: augmenting the training set with a specific subset of adversarial examples does not make the network immune to adversarial examples in general.

6. Conclusion

We are motivated by an oddity of CNNs: on the one hand they exhibit excellent generalization performance on difficult visual tasks, while on the other hand they exhibit an extreme sensitivity to adversarial examples. This sensitivity to adversarial examples suggests that these CNNs are not learning semantic concepts in the dataset. The goal of this article is to understand how a machine learning model can manage to generalize well without actually learning any high level semantics.

Drawing upon computer vision literature on the statistical regularity of natural images, we believe that it is pos-

sible for natural image training and test datasets to share many superficial cues. By learning these superficial cues, a machine learning model would be able to sidestep the issue of high level concept learning and generalize well. To this end, we posed our main hypothesis: *the current incarnation of deep neural networks have a tendency to learn surface statistical regularities as opposed to high level abstractions.*

To measure this tendency, we claim it is sufficient to construct a map F that perturbs a dataset in such a way that: 1) the recognizability of the objects/high level abstractions are almost entirely preserved from a human perspective while 2) the clean and perturbed datasets differ only in terms of their superficial statistical regularities. In this article, we show that appropriately tuned Fourier filtering satisfies these properties.

In our experimental results, we show that CNNs trained on a dataset with one class of Fourier image statistics in general do not generalize universally well to test distributions exhibiting qualitatively different types of Fourier image statistics. In some cases we are able to show an up to 28% gap in test accuracy. Furthermore, increasing the depth does not have a significant effect on closing this so-called generalization gap. We believe that this provides evidence for our main hypothesis.

While training on the fully augmented training set with the unfiltered and Fourier filtered datasets does have a significant impact on closing the generalization gap, we do not believe that this sort of data augmentation is sufficient for learning higher level abstractions in the dataset. It may be possible to generate some other perturbation of the dataset that yields a new generalization gap.

With respect to promising new directions to solve the high level abstraction learning problem, recent work like [42, 18] aim to learn good disentangled feature representations by combining unsupervised learning and reinforcement learning. In [16] a variational setup is used to learn visual concepts and [32] aims to learn abstract relations between objects in natural scene images. More generally, new proposals such as [2] aim to transition away from making predictions in the perceptual space and instead operate in the higher order abstract space. We believe these are all novel directions towards a deep neural architecture that can learn high level abstractions.

Acknowledgements

We would like to acknowledge the developers of Theano [41]. We would like to acknowledge the following organizations for their generous research funding and/or computational support (in alphabetical order): the CIFAR, Calcul Québec, Canada Research Chairs, Compute Canada, the IVADO and the NSERC.

References

- [1] Cifar-10 and cifar-100 datasets. <https://www.cs.toronto.edu/~kriz/cifar.html>. Accessed: 2017-11-04.
- [2] Y. Bengio. The consciousness prior. *CoRR*, abs/1709.08568, 2017.
- [3] E. O. Brigham. *The Fast Fourier Transform and Its Applications*. Prentice-Hall, Inc., Upper Saddle River, NJ, USA, 1988.
- [4] G. J. Burton and I. R. Moorhead. Color and spatial structure in natural scenes. *Appl. Opt.*, 26(1):157–170, Jan 1987.
- [5] M. Cisse, P. Bojanowski, E. Grave, Y. Dauphin, and N. Usunier. Parseval networks: Improving robustness to adversarial examples. In *Proceedings of The 34th International Conference on Machine Learning*, 2018.
- [6] A. Fawzi, O. Fawzi, and P. Frossard. Analysis of classifiers’ robustness to adversarial perturbations. *CoRR*, abs/1502.02590, 2015.
- [7] D. J. Field. Relations between the statistics of natural images and the response properties of cortical cells. *J. Opt. Soc. Am. A*, 4(12):2379–2394, Dec 1987.
- [8] R. E. Galper. Recognition of faces in photographic negative. *Psychonomic Science*, 19(4):207–208, Oct 1970.
- [9] I. J. Goodfellow, J. Shlens, and C. Szegedy. Explaining and harnessing adversarial examples. In *Proceedings of the International Conference on Learning Representations (ICLR)*, 2015.
- [10] R. Gopalan, R. Li, and R. Chellappa. Domain adaptation for object recognition: An unsupervised approach. In *2011 International Conference on Computer Vision*, pages 999–1006, Nov 2011.
- [11] S. Gu and L. Rigazio. Towards deep neural network architectures robust to adversarial examples. In *ICLR Workshop*, 2015.
- [12] T. Hayes, M. C. Morrone, and D. C. Burr. Recognition of positive and negative bandpass-filtered images. *Perception*, 15(5):595–602, 1986. PMID: 3588219.
- [13] K. He, X. Zhang, S. Ren, and J. Sun. Delving deep into rectifiers: Surpassing human-level performance on imagenet classification. In *Proceedings of the 2015 IEEE International Conference on Computer Vision (ICCV), ICCV ’15*, pages 1026–1034, Washington, DC, USA, 2015. IEEE Computer Society.
- [14] K. He, X. Zhang, S. Ren, and J. Sun. Deep residual learning for image recognition. In *2016 IEEE Conference on Computer Vision and Pattern Recognition (CVPR)*, pages 770–778, June 2016.
- [15] K. He, X. Zhang, S. Ren, and J. Sun. *Identity Mappings in Deep Residual Networks*, pages 630–645. Springer International Publishing, Cham, 2016.
- [16] I. Higgins, N. Sonnerat, L. Matthey, A. Pal, C. Burgess, M. Botvinick, D. Hassabis, and A. Lerchner. SCAN: learning abstract hierarchical compositional visual concepts. *CoRR*, abs/1707.03389, 2017.
- [17] H. Hosseini and R. Poovendran. Deep neural networks do not recognize negative images. *CoRR*, abs/1703.06857, 2017.
- [18] M. Jaderberg, V. Mnih, W. M. Czarnecki, T. Schaul, J. Z. Leibo, D. Silver, and K. Kavukcuoglu. Reinforcement learning with unsupervised auxiliary tasks. *CoRR*, abs/1611.05397, 2016.
- [19] J. Kovacevic and A. Chebira. *An Introduction to Frames*. Now Publishers Inc., Hanover, MA, USA, 2008.
- [20] A. Kurakin, I. J. Goodfellow, and S. Bengio. Adversarial machine learning at scale. *CoRR*, abs/1611.01236, 2016.
- [21] Y. Lecun, L. Bottou, Y. Bengio, and P. Haffner. Gradient-based learning applied to document recognition. *Proceedings of the IEEE*, 86(11):2278–2324, Nov 1998.
- [22] T. Miyato, S. ichi Maeda, M. Koyama, K. Nakae, and S. Ishii. Distributional smoothing with virtual adversarial training. In *ICLR*, 2016.
- [23] S. Moosavi-Dezfooli, A. Fawzi, O. Fawzi, and P. Frossard. Universal adversarial perturbations. In *CVPR*, 2017.
- [24] S. M. Moosavi Dezfooli, A. Fawzi, and P. Frossard. DeepFool: a simple and accurate method to fool deep neural networks. In *Proceedings of 2016 IEEE Conference on Computer Vision and Pattern Recognition (CVPR)*, 2016.
- [25] Y. Nesterov. A method of solving a convex programming problem with convergence rate $O(1/\sqrt{k})$. *Soviet Mathematics Doklady*, 27:372–376, 1983.
- [26] Y. Netzer, T. Wang, A. Coates, A. Bissacco, B. Wu, and A. Y. Ng. Reading digits in natural images with unsupervised feature learning. In *NIPS Workshop on Deep Learning and Unsupervised Feature Learning 2011*, 2011.
- [27] A. Nguyen, J. Yosinski, and J. Clune. Deep neural networks are easily fooled: High confidence predictions for unrecognizable images. 2015.
- [28] N. Papernot, P. McDaniel, X. Wu, S. Jha, and A. Swami. Distillation as a defense to adversarial perturbations against deep neural networks. In *2016 IEEE Symposium on Security and Privacy (SP)*, pages 582–597, May 2016.
- [29] D. E. Pearson and J. A. Robinson. Visual communication at very low data rates. *Proceedings of the IEEE*, 73(4):795–812, April 1985.
- [30] R. J. Phillips. Why are faces hard to recognize in photographic negative? *Perception and Psychophysics*, 12(5):425–428, 1972.
- [31] N. Pinto, Y. Barhomi, D. D. Cox, and J. J. DiCarlo. Comparing state-of-the-art visual features on invariant object recognition tasks. In *2011 IEEE Workshop on Applications of Computer Vision (WACV)*, pages 463–470, Jan 2011.
- [32] D. Raposo, A. Santoro, D. G. T. Barrett, R. Pascanu, T. P. Lillicrap, and P. W. Battaglia. Discovering objects and their relations from entangled scene representations. *CoRR*, abs/1702.05068, 2017.
- [33] A. Rozsa, M. Günther, and T. E. Boult. Towards robust deep neural networks with BANG. *CoRR*, abs/1612.00138, 2016.
- [34] O. Russakovsky, J. Deng, H. Su, J. Krause, S. Satheesh, S. Ma, Z. Huang, A. Karpathy, A. Khosla, M. Bernstein, A. C. Berg, and L. Fei-Fei. ImageNet Large Scale Visual Recognition Challenge. *International Journal of Computer Vision (IJCV)*, 115(3):211–252, 2015.
- [35] K. Saenko, B. Kulis, M. Fritz, and T. Darrell. *Adapting Visual Category Models to New Domains*, pages 213–226. Springer Berlin Heidelberg, Berlin, Heidelberg, 2010.

- [36] U. Shaham, Y. Yamada, and S. Negahban. Understanding adversarial training: Increasing local stability of neural nets through robust optimization. *CoRR*, abs/1511.05432, 2015.
- [37] L. Shao, F. Zhu, and X. Li. Transfer learning for visual categorization: A survey. *IEEE Transactions on Neural Networks and Learning Systems*, 26(5):1019–1034, May 2015.
- [38] H. C. Shin, H. R. Roth, M. Gao, L. Lu, Z. Xu, I. Nogues, J. Yao, D. Mollura, and R. M. Summers. Deep convolutional neural networks for computer-aided detection: Cnn architectures, dataset characteristics and transfer learning. *IEEE Transactions on Medical Imaging*, 35(5):1285–1298, May 2016.
- [39] J. Stallkamp, M. Schlipsing, J. Salmen, and C. Igel. Man vs. computer: Benchmarking machine learning algorithms for traffic sign recognition. *Neural Networks*, 32(Supplement C):323 – 332, 2012. Selected Papers from IJCNN 2011.
- [40] C. Szegedy, W. Zaremba, I. Sutskever, J. Bruna, D. Erhan, I. J. Goodfellow, and R. Fergus. Intriguing properties of neural networks. *CoRR*, abs/1312.6199, 2013.
- [41] Theano Development Team. Theano: A Python framework for fast computation of mathematical expressions. *arXiv e-prints*, abs/1605.02688, May 2016.
- [42] V. Thomas, J. Pondard, E. Bengio, M. Sarfati, P. Beaudoin, M. Meurs, J. Pineau, D. Precup, and Y. Bengio. Independently controllable factors. *CoRR*, abs/1708.01289, 2017.
- [43] A. Torralba and A. Oliva. Statistics of natural image categories. *Network: Computation in Neural Systems*, 14:391–412, 2003.
- [44] J. Yosinski, J. Clune, Y. Bengio, and H. Lipson. How transferable are features in deep neural networks? In *Proceedings of the 27th International Conference on Neural Information Processing Systems - Volume 2*, NIPS’14, pages 3320–3328, Cambridge, MA, USA, 2014. MIT Press.
- [45] S. Zagoruyko and N. Komodakis. Wide residual networks. In *BMVC*, 2016.

A. Additional Fourier Filtered Images

A.1. SVHN

In Figure 9 we present more pictures of Fourier filtered SVHN images. We present a random mask which can result in color deformations. We show 2 randomly chosen images for each label.

A.2. CIFAR-10

In Figure 10 we present more pictures of Fourier filtered CIFAR-10 images. We present a random mask which can result in color deformations. We show 2 randomly chosen images for each label.

B. Preact-ResNet-92 Experimental Plots

In this section we share our Preact-ResNet-92 graphical plots.



Figure 9: The first image in each row corresponds to the Fourier mask in frequency space. A white pixel corresponds to preserving the Fourier mode, black/color corresponds to setting it to zero. Best viewed in color.

B.1. SVHN

In Figures 11 and 12 we show the Preact-ResNet-92 plots for the SVHN datasets.

B.2. CIFAR-10

In Figures 13 and 14 we show the Preact-ResNet-92 plots for the SVHN datasets.

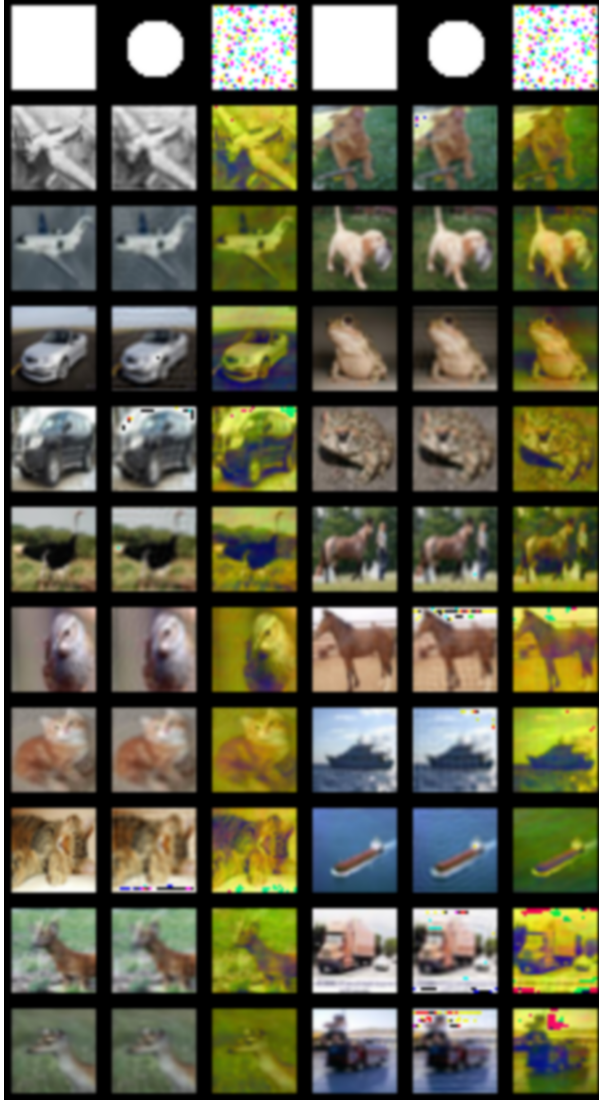


Figure 10: The first image in each row corresponds to a Fourier mask in frequency space. A white pixel corresponds to preserving the Fourier mode, black/color corresponds to setting it to zero. Best viewed in color.

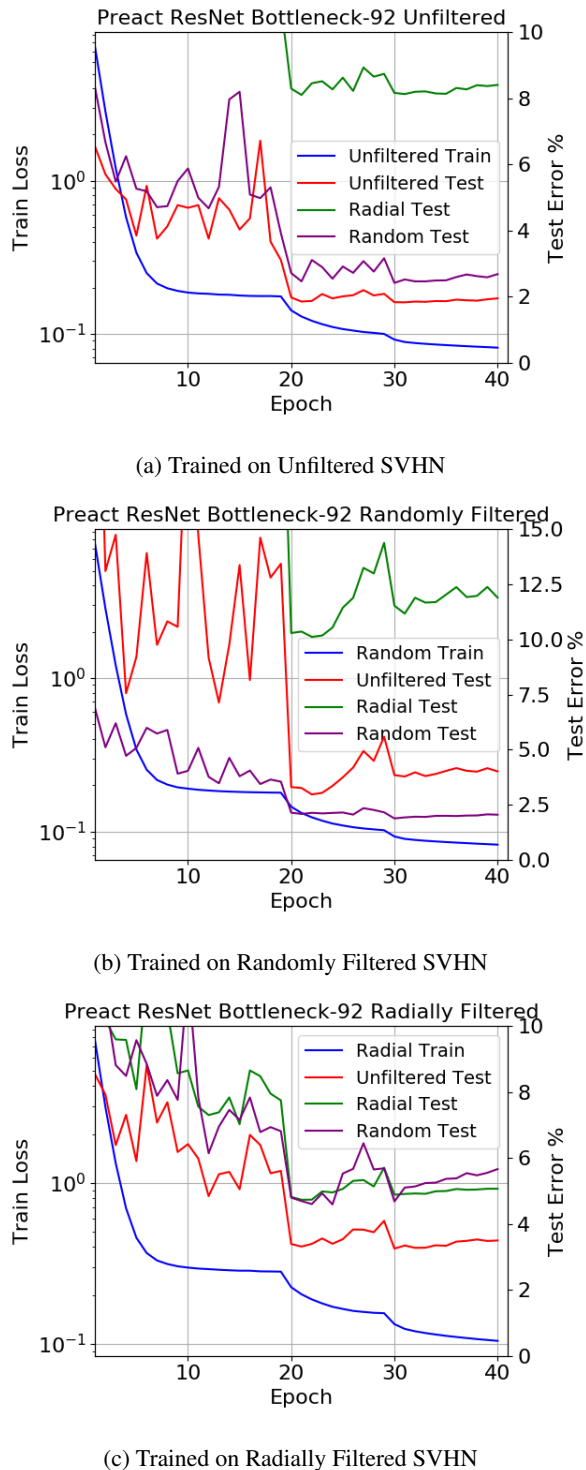


Figure 11: Generalization plots for Preact-ResNet-Bottleneck-92 model. (a) Trained on unfiltered SVHN. (b) Trained on randomly filtered SVHN data. (c) Trained on radially filtered SVHN data. Best viewed in color.

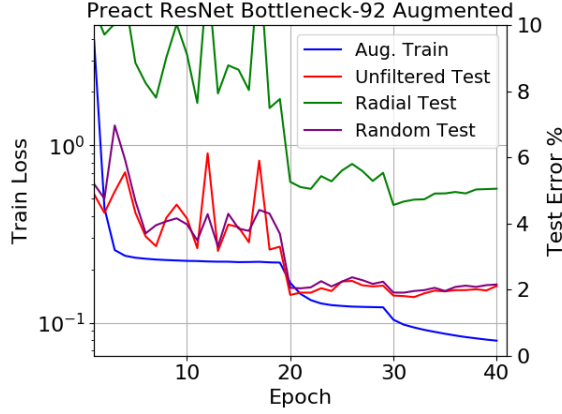
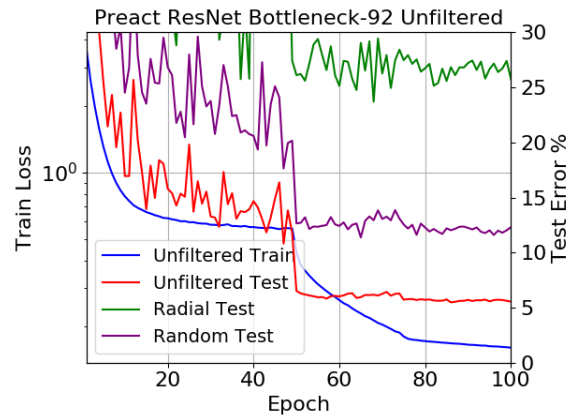
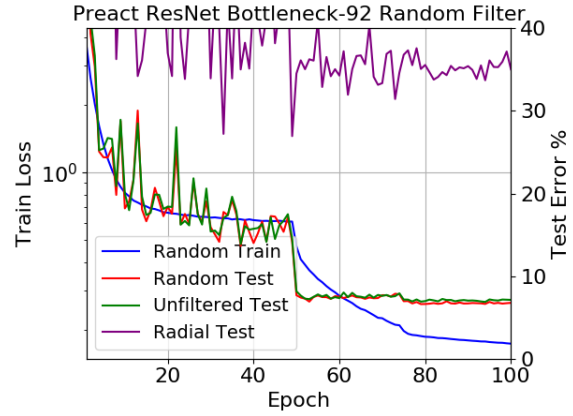


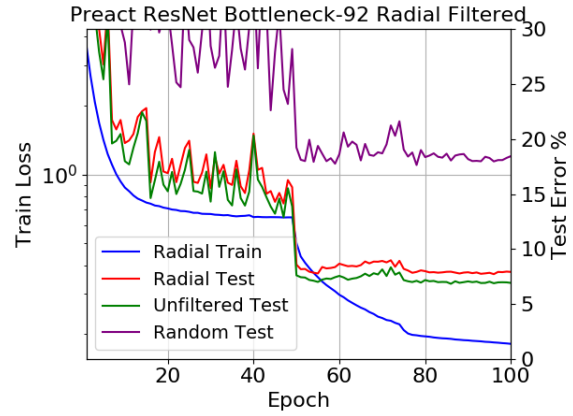
Figure 12: Preact-ResNet-92 Trained on Fully Augmented SVHN. Best reviewed in color.



(a) Trained on Unfiltered CIFAR-10



(b) Trained on Randomly Filtered CIFAR-10



(c) Trained on Radially Filtered CIFAR-10

Figure 13: Generalization plots for Preact-ResNet-Bottleneck-92 model. (a) Trained on unfiltered CIFAR-10 data. (b) Trained on randomly filtered CIFAR-10 data. (c) Trained on radially filtered CIFAR-10 data. Best viewed in color.

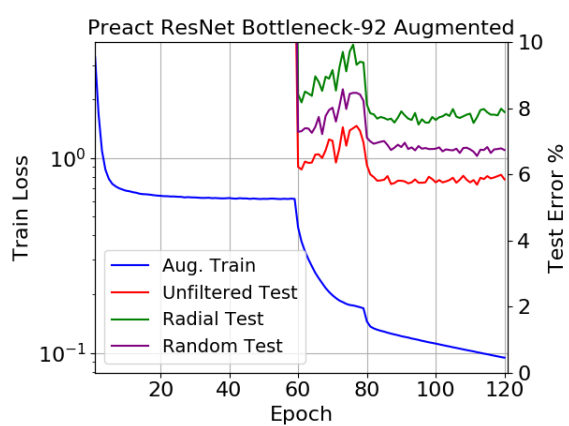


Figure 14: Preact-ResNet-92 Trained on Fully Augmented CIFAR-10. Best viewed in color.